FOXO1 Deletion Reverses the Effect of Diabetic-Induced Impaired Fracture Healing

Mohammed A. Alharbi,[1] Citong Zhang,[2] Chanyi Lu,[2] Tatyana N. Milovanova,[2] Leah Yi,[3] Je Dong Ryu,[2] Hongli Jiao,[2] Guangyu Dong,[2] J. Patrick O'Connor,[4] and Dana T. Graves[2]

Diabetes 2018;67:2682–2694 | https://doi.org/10.2337/db18-0340

Type 1 diabetes impairs fracture healing. We tested the hypothesis that diabetes affects chondrocytes to impair fracture healing through a mechanism that involves the transcription factor FOXO1. Type 1 diabetes was induced by streptozotocin in mice with FOXO1 deletion in chondrocytes (Col2α1Cre^{+}.FOXO1$^{L/L}$) or littermate controls (Col2α1Cre^{-}.FOXO1$^{L/L}$) and closed femoral fractures induced. Diabetic mice had 77% less cartilage and 30% less bone than normoglycemics evaluated histologically and by micro-computed tomography. Both were reversed with lineage-specific FOXO1 ablation. Diabetic mice had a threefold increase in osteoclasts and a two- to threefold increase in RANKL mRNA or RANKL-expressing chondrocytes compared with normoglycemics. Both parameters were rescued by FOXO1 ablation in chondrocytes. Conditions present in diabetes, high glucose (HG), and increased advanced glycation end products (AGEs) stimulated FOXO1 association with the RANKL promoter in vitro, and overexpression of FOXO1 increased RANKL promoter activity in luciferase reporter assays. HG and AGE stimulated FOXO1 nuclear localization, which was reversed by insulin and inhibitors of TLR4, histone deacetylase, nitric oxide, and reactive oxygen species. The results indicate that chondrocytes play a prominent role in diabetes-impaired fracture healing and that high levels of glucose, AGEs, and tumor necrosis factor-α, which are elevated by diabetes, alter RANKL expression in chondrocytes via FOXO1.

Long bone fracture healing is a dynamic process that involves sophisticated and coordinated activities of stem cells, inflammatory cells, chondrocytes, osteoblasts, osteoclasts, and other cell types (1). It requires recruitment, proliferation, and differentiation of undifferentiated mesenchymal stem cells into cartilage-producing chondrocytes, which produce cartilage to form a callus that stabilizes the fractured bone (2). It has been shown via lineage tracing that skeletal progenitor cells during fracture healing originate from the periosteum and/or bone marrow/endosteal cells during fracture repair (3). The callus cartilage is calcified, resorbed, and replaced by bone. Initially, chondrocytes proliferate and then express type II collagen and other proteins that form the cartilaginous matrix and signaling factors (4). Chondrocytes will then mature to a hypertrophic phase characterized by expressing type X collagen (5). Calcified cartilage matrix undergoes degradation by osteoclasts, and it is associated with invasion by blood vessels (6). Although some of the chondrocytes undergo apoptosis, recent evidence indicates that others may transdifferentiate to osteoblasts to form bone (7,8).

There are >6 million fractures annually in the U.S., with 10–15% significantly delayed or with healing that is impaired by formation of nonunions (9). Type 1 diabetes is a significant risk for negative outcomes (10), which has increased 2–3% yearly since 2000 (11,12). As a result of improved treatment, people with diabetes live longer, but impaired fracture healing remains a significant orthopedic challenge despite the availability of insulin (13,14). It has been suggested that the prolonged hyperglycemic status in addition to the upregulation of oxidative stress negatively affect the fracture healing in individuals with diabetes. A considerable effort has been made to identify the impact of diabetes on osteoblasts and bone formation (15–17). However, less attention has been paid to

[1]Department of Endodontics, Faculty of Dentistry, King Abdulaziz University, Jeddah, Saudi Arabia
[2]Department of Periodontics, School of Dental Medicine, University of Pennsylvania, Philadelphia, PA
[3]Department of Orthodontics, School of Dental Medicine, University of Pennsylvania, Philadelphia, PA
[4]Department of Orthopedics, New Jersey Medical School, Rutgers University, Newark, NJ

Corresponding author: Dana T. Graves, dtgraves@upenn.edu.

Received 21 March 2018 and accepted 21 September 2018.

chondrocytes and their contribution to diabetes-impaired fracture healing.

FOXO1 is a member of the forkhead transcription factor family, and it is important for the regulation of cellular processes, including apoptosis, oxidative stress, and proliferation (18). FOXO1 expression is found in both bone and cartilage and is the most studied and abundant FOXO member in bone (18,19). In chondrocytes, knockdown of FOXO1 has a major effect, whereas knockdown of a related FOXO member, FOXO3, has less impact (19). It has previously been shown that FOXO1 is significantly elevated in diabetic fractures and that diabetic fracture is characterized by the premature loss of cartilage. However, the role of FOXO1 in fracture healing has not been established. To address whether FOXO1 activation in chondrocytes represents an important mechanism for altered diabetic fracture healing, we examined mice with lineage-specific FOXO1 deletion. The results indicate that chondrocytes play a primary role in the premature loss of cartilage that occurs in diabetic fracture healing through a mechanism that involves FOXO1-regulated RANKL expression.

RESEARCH DESIGN AND METHODS

Animals and Induction of Diabetes

The *Guide for the Care and Use of Laboratory Animals*, eighth edition (2011), was followed, and all animal experiments were approved and conducted in conformity with the University of Pennsylvania Institutional Animal Care and Use Committee. Twelve- to 14-week-old Col2α1Cre^{+}.FOXO1$^{L/L}$ mice with lineage-specific FOXO1 deletion in chondrocytes were used as the experimental group, and results were compared with Col2α1Cre^{-}.FOXO1$^{L/L}$ littermate controls. Two to five mice were housed per cage under standard conditions with 14-h light/10-h dark cycles. To confirm the presence or absence of Cre recombinase in the animals, genotyping was performed via PCR using both Cre and FOXO1 primers. Genomic DNA was obtained from the mice's ears or tails before starting the experiment, and the results were validated at the time of euthanasia (Fig. 1*A*). Mice were rendered type 1 diabetic as described by us (20) and originally by Like and Rossini (21). Intraperitoneal streptozotocin injections (40 mg/kg in 10 mmol/L citrate buffer) (Sigma-Aldrich, St. Louis, MO) were performed once every day for 5 consecutive days. Control mice received vehicle alone. Blood glucose levels were measured weekly 10 days after the last injection. Mice were considered diabetic when their blood glucose levels were >220 mg/dL for two consecutive readings. Experiments were initiated when mice had been diabetic for at least 3 weeks.

Femoral Fractures

An incision was made lateral to the knee, and the patella was pushed laterally to expose the articular surface of the femur. A 27-gauge needle was used to gain access to the medullary canal, and then a 30-gauge spinal needle was inserted for fixation. After suturing the incision, a controlled, closed, simple, transverse fracture was created by blunt trauma as we have described (22). Animals were euthanized, and femurs were harvested at 10, 16, and 22 days after fracture. Fractures were evaluated physically and radiographically after euthanasia. Fractures that were not middiaphyseal or that were grossly comminuted were excluded from the study.

Histology and Histomorphometric Analysis

Samples were fixed for 24 h in cold 4% paraformaldehyde and then decalcified for 5 weeks by incubation at room temperature 10% EDTA solution before embedding in paraffin blocks. Transverse sections were prepared as described by us and initially by Gerstenfeld et al. (22) and Kayal et al. (23). Safranin-O/fast green–stained sections were measured for total callus within the peripheral fibrous capsule excluding the original cortical bone, bone, and cartilage areas. Each tissue was assessed using computer-assisted image analysis (NIS element software; Nikon, Tokyo, Japan). Multinucleated osteoclasts lining the cartilage surface were identified by tartrate-resistant acid phosphatase (TRAP) staining and by immunohistochemistry with anti–cathepsin K antibody as described below.

Micro-Computed Tomography and Image Analysis

The fractured femurs were scanned using a desktop micro-computed tomography (micro-CT) system Viva CT40 (Scanco Medical, Brüttisellen, Switzerland) at 19-μm voxel size. Scan settings were 70 kVp, 114 mA, and 200-ms integration time. Noise reduction was accomplished using a constrained, three-dimensional Gaussian filter (σ = 0.8, support = 1). A fixed global threshold was chosen that represented the transition in X-ray attenuation between mineralized and unmineralized tissue. The three-dimensional reconstructions were done using the Viva CT40 software at the same threshold. Segmentation and countering were achieved manually on a slice-by-slice basis, and the parameters total volume and bone volume were measured as described in Bouxsein et al. (24).

Immunofluorescence and Immunohistochemistry of Histologic Sections

Paraffin sections were dewaxed, and antigen retrieval was performed at 120°C in 10 mmol/L citric acid, pH 6.0 (2100-Retriever; Aptum, Southampton, U.K.) for 20 min followed by nonspecific blocking with nonimmune serum matching the secondary antibody for 55 min. Sections were incubated overnight at 4°C with anti-FOXO1 antibody (1:200) (sc-11350; Santa Cruz Biotechnology, Dallas, TX), anti-RANKL antibody (1:100) (sc9073; Santa Cruz Biotechnology), anti–cathepsin K antibody (1:400) (ab19027; Abcam, Cambridge, U.K.), or the appropriate isotype-matched negative control IgG with the concentration adjusted to match the primary antibody (Cell Signaling Technology, Danvers, MA). Sections were then incubated with a biotinylated secondary antibody (1:200) (Vector Laboratories, Burlingame, CA) followed by avidin-biotin-peroxidase enzyme

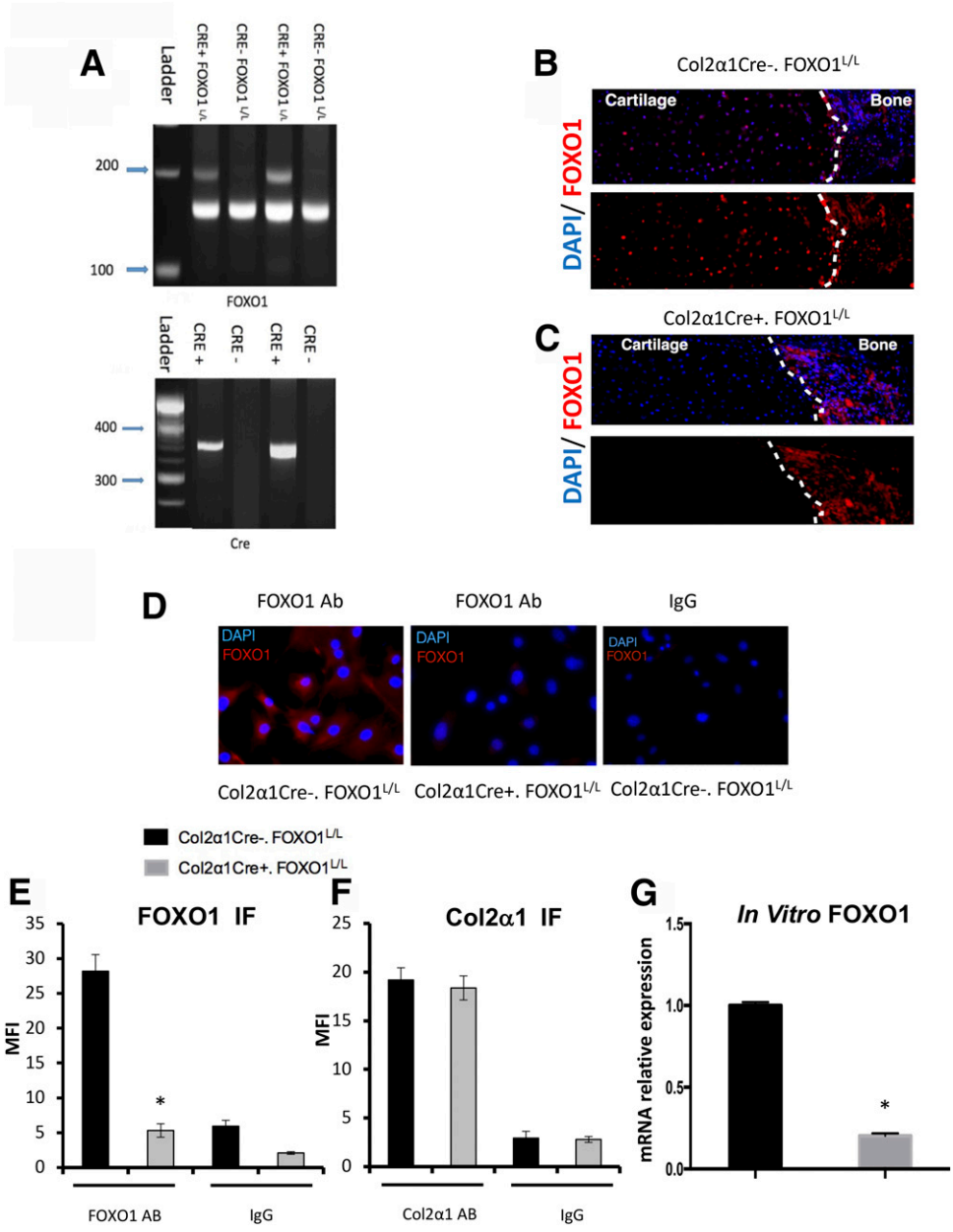

Figure 1—Cre recombinase deletes FOXO1 in chondrocytes of Col2α1Cre^{+}.FOXO$^{L/L}$ but not control Col2α1Cre^{-}.FOXO$^{L/L}$ mice. *A*: Genotyping of experimental and littermate control mice. *FOXO1* with flanking loxP sites (149 bp) is detected in all groups, whereas cleaved *FOXO1* (198 bp) is found only in experimental mice with Cre recombinase (352 bp). *B* and *C*: Photomicrographs of histologic sections from the fracture site were examined by immunofluorescence with antibody specific for FOXO1, and nuclei were identified by DAPI counterstain. No signal was detected in matched control antibody. The white dotted line indicates the interface between cartilage and bone. Original magnification ×100. *D*: Photomicrographs of primary chondrocytes isolated from experimental Col2α1Cre^{+}.FOXO1$^{L/L}$ and littermate control Col2α1Cre^{-}.FOXO1$^{L/L}$ mice. Immunofluorescence (IF) was carried out with antibody (AB) specific to FOXO1 or control IgG. Magnification ×400. *E*: Mean fluorescence intensity (MFI) was measured from specimens described in *D*. *F*: Primary chondrocytes were isolated from experimental Col2α1Cre^{+}.FOXO1$^{L/L}$ (knockout) and littermate control Col2α1Cre^{-}.FOXO1$^{L/L}$ mice. Immunofluorescence was carried out with antibody specific to collagen-2α1, a chondrocyte marker, or control IgG, and MFI was measured. *G*: Primary chondrocytes were isolated from the control Col2α1Cre^{-}.FOXO1$^{L/L}$ and experimental Col2α1Cre^{+}.FOXO1$^{L/L}$ mice and grown to confluence. They were then cultured in chondrogenic media for 4 days. RNA was obtained, and FOXO1 mRNA levels were measured by real-time PCR to quantify the knockdown efficacy. Quantitative data are expressed as the mean ± SEM. *Significant difference between specimens from Col2α1Cre^{+}.FOXO1$^{L/L}$ and littermate control Col2α1Cre^{-}.FOXO1$^{L/L}$ mice determined by Student *t* test ($P < 0.05$).

complex (PK-4000; Vector Laboratories), which was localized with 3,3′-diaminobenzidine chromogen or Alexa Fluor 546–conjugated streptavidin (1:400) (S-11225; Invitrogen, Carlsbad, CA) followed by mounting with DAPI-containing mounting media (Sigma-Aldrich). Tyramide signal amplification (1:50) (CDX-B0270-M100; Adipogen) was used to enhance the signal. Images were captured with a Nikon Eclipse 90i microscope equipped for epifluorescence.

The exposure time was set to the experimental group based on the IgG control signals. The percentage of RANKL-positive cells for each slide was obtained by dividing the number of Alexa Fluor 546–positive cells by the number of DAPI-positive cells. Cathepsin K–positive osteoclasts were counted.

RANKL mRNA Quantitative PCR

Different sets of animals, five to six per group, were used for real-time PCR analysis 10 days postfracture. After euthanasia, the fracture calluses were dissected from the femurs. All of the muscles and noncallus tissues were removed, and the samples were immediately frozen in liquid nitrogen. Total RNA was extracted using RNAqueous (Ambion, Waltham, MA) following the manufacturer's instructions. Reverse transcription was performed using High-Capacity RNA-to-cDNA Kit (Applied Biosystems, Foster City, CA). mRNA levels of RANKL were measured in triplicate using the StepOnePlus Real-Time PCR System (Thermo Fisher Scientific, Waltham, MA). Results were normalized with the housekeeping gene RPL32, a ribosomal protein. Results obtained from the animals within the same group were combined to derive mean values.

Primary Cell Culture

Primary costal chondrocytes were isolated from 2–4-day-old experimental Col2α1Cre^{+}.FOXO1$^{L/L}$ and control Col2α1Cre^{-}.FOXO1$^{L/L}$ mice as described before in (25). Briefly, ribs were isolated, washed with PBS, incubated in Pronase (Thermo Fisher Scientific) for 45 min at 37°C to dissolve the soft tissue, and then they were washed with PBS followed by a 60-min incubation in Collagenase D (Thermo Fisher Scientific) to dissociate the hard tissue from the remaining soft tissues. Ribs were then incubated in collagenase D for 3–5 h at 37°C and released cells separated from debris with a 70-μm strainer and incubated in DMEM media supplemented with 10% FBS and 1% Antibiotic-Antimycotic (Anti-Anti; Thermo Fisher Scientific). All cell cultures were maintained in a 5% CO_2 humidified incubator at 37°C.

In Vitro Immunofluorescence

Primary chondrocytes isolated from experimental Col2α1Cre^{+}.FOXO1$^{L/L}$ and control Col2α1Cre^{-}.FOXO1$^{L/L}$ were seeded in 96-well plates and incubated in standard media (DMEM supplemented with 10% FBS and 1% Anti-Anti) containing 5 mmol/L D-glucose (low glucose) for 5 days, to serve as a control, or supplemented to 25 mmol/L D-glucose (high glucose [HG]) for 5 days. Cells were also incubated with 200 μg/mL carboxymethyllysine-modified BSA (CML-BSA) for 3 days, prepared as previously described (26), or unmodified BSA (Sigma-Aldrich) for 3 days. Cells were fixed for 10 min with 3.7% formaldehyde, permeabilized in 0.5% Triton X-100 for 5 min, incubated with 2% BSA, and incubated with primary anti-RANKL antibody (1:100) (sc9073; Santa Cruz Biotechnology); control cells were stained with anti-Col2α1 antibody (1:200) (sc-7764; Santa Cruz Biotechnology) or anti-FOXO1 antibody (1:200) (sc-11350; Santa Cruz Biotechnology) to confirm the cells' phenotypes and confirm the lineage-specific deletion of FOXO1 (Fig. 1*D–F*). Primary antibody was detected with biotinylated secondary antibody and Alexa Fluor 546–conjugated streptavidin followed by mounting with DAPI-containing mounting media. Images were captured by a fluorescence microscope (Nikon Eclipse Ti; Boston Industries, Inc., Walpole, MA) with the same exposure time for both the control and the experimental group. The mean fluorescence intensity for RANKL expression was measured using NIS Elements AR image analysis software (Nikon).

In Vitro RANKL Expression

Primary chondrocytes isolated from experimental Col2α1Cre^{+}.FOXO1$^{L/L}$ and control Col2α1Cre^{-}.FOXO1$^{L/L}$ were seeded in 96-well plates. Cells were incubated for 2 days in low serum media (0.5%) followed by either 10% serum stimulation for 14 h or hypertrophic differentiation induction for 4 days using DMEM with 10% FBS supplemented with 10 mmol/L β-glycerophosphate and 50 μg/mL ascorbic acid (25). RNA was extracted from the chondrocytes using the Quick-RNA Microprep kit (Zymo, Irvine, CA) and RANKL mRNA measured by real-time PCR.

Chromatin Immunoprecipitation Assay

Chromatin immunoprecipitation (ChIP) assays were carried out with the ChIP-IT Kit (Active Motif, Carlsbad, CA) using ~1.5×10^7 ATDC5 murine chondrocytes. The ATDC5 were cultured using different conditions, which included: *1*) hypertrophic differentiation for 6 days using a 1:1 mixture of DMEM and Ham's F12 medium supplemented with 5% FBS, 1% Anti-Anti, 50 μg/mL ascorbic acid, and 0.5 mmol/L NaH_2PO_4, *2*) cells at 70–80% treated with CML-BSA (200 μg/mL) for 3 days or unmodified BSA (200 μg/mL) for 3 days, and *3*) cells grown in HG (25 mmol/L) media for 5 days or mannitol (25 mmol/L) as osmotic control. Cells were fixed with formaldehyde and nuclei obtained following Dounce homogenization. ChIP was performed following the manufacturer's instructions using an anti-FOXO1 antibody (5 μg) (SC-11350X; Santa Cruz Biotechnology) or control polyclonal nonspecific IgG (Cell Signaling Technology). Chromatin–antibody complexes were purified using protein G–coupled beads. Three quantitative real-time PCR reactions for the RANKL gene promoter with primers used were: forward, 5′-TGAAGA CACACTACCTGACTCCTG-3′ and reverse, 5′-CCCACAAT GTGTTGCAGTTC-3′, which flanks a consensus *FOXO1* response element. The experiment was repeated three times with similar results.

Luciferase Reporter Assay

Transient transfection with luciferase reporter constructs was performed using Lipofectamine 3000 (Thermo Fisher Scientific) in 48-well plates as described (27). Briefly, ATDC5 cells were cultured in DMEM/F12 (1:1) media supplemented with 0.5% FBS and 1% Anti-Anti. At 70% confluence, they were incubated in standard or HG media (25 mmol/L) for 5 days or standard media plus BSA or

CML-BSA (200 μg/mL) for 3 days. Cells were cotransfected with a RANKL luciferase reporter (provided by Dr. C. A. O'Brien, the University of Arkansas for Medical Sciences, Little Rock, AR) (28) together with pGL3 luciferase control vector, a constitutively active FOXO1 expression plasmid, FOXO1-ADA (Addgene), or pCMV control plasmid. Two days after transfection, cells were lysed, and Firefly and Renilla luciferase activities were measured using the Dual-Luciferase Reporter Assay kit (Promega, Madison, WI) according to the manufacturer's instructions. Experiments were performed two to three times with similar results.

FOXO1 Nuclear Localization

ATDC5 chondrocytes were incubated in media as described above and at 70% confluence were incubated in low glucose or HG (25 mmol/L D-glucose) for 5 days or CML-BSA (200 μg/mL) or unmodified BSA for 3 days with 0.5% FBS. The following inhibitors or insulin were added 24 h before the lysis of the cells: 1L6-hydroxymethyl-chiro-inositol-2-(R)-2-*O*-methyl-3-*O*-octadecyl-sn-glycerocarbonate, an AKT inhibitor (10 μmol/L) (catalog number 124005; EMD Millipore, Burlington, MA); TAK242, a TLR4 inhibitor (5 μmol/L) (Millipore Sigma); trichostatin A, a deacetylase inhibitor (25 nmol/L) (89730; Cayman Chemical Company, Ann Arbor, MI); *N*-acetyl-L-cysteine (NAC), an antioxidant (2.5 μmol/L) (A9165; Sigma-Aldrich); L-N^G-nitro-L-arginine methyl ester hydrochloride (L-NAME), a nitric oxide synthase inhibitor (0.5 mmol/L) (N5751; Sigma-Aldrich); and insulin (10 μg/mL) (I9278; Sigma-Aldrich). As a positive control, cells were incubated with murine tumor necrosis factor-α (TNF-α; 10 ng/mL) (PeproTech, Rocky Hill, NJ) for 1 h. Nuclear localization of FOXO1 was measured by flow cytometry. Cells were fixed with 4% paraformaldehyde, permeabilized with 100% methanol (−20°C), and incubated with FOXO1 anti-mouse phycoerythrin-conjugated mAb (14262S; Cell Signaling Technology, Beverly, MA) for 30 min at 4°C. Cells were lysed with Vindelov reagent and nuclei counterstained with DRAQ5 (51-9011170; BD Pharmingen, Franklin Lakes, NJ). FACS analysis was performed on an LSR II FACS computer (BD Biosciences, San Jose, CA), and the data were analyzed with FlowJo software, version 10.7 (Tree Star, Ashland, OR).

Statistics

Unless otherwise stated, data were analyzed by one-way ANOVA and differences between groups determined using Tukey post hoc tests. In some in vitro experiments, only two groups were compared, and Student *t* test was used. A P value <0.05 was considered statistically significant. Data are expressed as the mean ± SD.

RESULTS

Lineage-Specific FOXO1 Deletion Reverses the Impact of Diabetes on Reduced Cartilage, Callus Size, and Bone

Histomorphometry was performed on fracture calluses from normoglycemic Col2α1-Cre^-.$FOXO1^{L/L}$ control, diabetic control mice, and diabetic mice with targeted loss of FOXO1 in chondrocytes, Col2α1Cre^+.$FOXO1^{L/L}$. Cartilage, callus, and bone were measured at the fracture midline in histologic sections stained with Safranin-O and fast green (Fig. 2*A*–*C*). Although 10 days after fracture, by day 16, the diabetic group had 77% less cartilage than the normoglycemic group ($P < 0.05$) (Fig. 2*D*). FOXO1 ablation in chondrocytes of diabetic mice prevented the loss of cartilage noted on day 16 ($P < 0.05$) (Fig. 2*D*). The deletion of FOXO1 in chondrocytes had a subsequent effect on total callus size and bone formation. Diabetic mice had 43% smaller calluses on day 16 and 37% smaller on day 22 compared with the normoglycemic control group ($P < 0.05$) (Fig. 2*D*). Chondrocyte-specific deletion of FOXO1 in diabetic mice rescued the deficit at both time points (Fig. 2*D*). Additionally, the bone area on days 16 and 22 was ∼50% smaller in diabetic mice compared with normoglycemic controls ($P < 0.05$) (Fig. 1*D*). The negative effect of diabetes on new bone formation was largely reversed when FOXO1 was ablated in chondrocytes of diabetic experimental mice ($P < 0.05$) (Fig. 2*D*).

Similar results were obtained by micro-CT analysis of the mouse fracture calluses. On day 16 and 22 postfracture, total callus and bone volume were ∼30–45% smaller in the diabetic compared with the normoglycemic group ($P < 0.05$) (Fig. 3*D*). Both total callus volume and bone volume were restored to normal levels in the diabetic Col2α1Cre^+.$FOXO1^{L/L}$ mice compared with diabetic littermate controls at both time points (Fig. 3*D*). There was no statistically significant difference between the normoglycemic control group and normoglycemic mice with FOXO1 deletion at both time points (Fig. 3*D*).

FOXO1 Deletion Rescues Diabetes-Enhanced Osteoclast Numbers

The effect of diabetes and targeted deletion of FOXO1 on osteoclasts was measured by counting $TRAP^+$ cells lining the cartilage surface (Fig. 4*A*–*D*). At day 10 after fracture, there was a 182% increase in cartilage-associated osteoclasts in the diabetic group compared with normoglycemic littermate controls ($P < 0.05$) (Fig. 4*E*). The increase in osteoclasts lining cartilage induced by diabetes was blocked by targeted deletion of FOXO1 in chondrocytes so that the number was similar to that in the normoglycemic mice ($P < 0.05$) (Fig. 4*E*). Furthermore, immunohistochemistry with cathepsin K–specific antibody validated the results obtained from the TRAP histostain. Diabetes significantly increased the number of cathepsin K–positive osteoclasts lining cartilage ($P < 0.05$), and lineage-specific FOXO1 deletion reduced the number to one that was comparable to the normoglycemic controls ($P > 0.05$) (Fig. 4*E*).

FOXO1 Regulates RANKL Expression

To assess expression of RANKL in chondrocytes in vivo, histologic sections were examined by immunofluorescence and the number of chondrocytes expressing RANKL counted. Calluses from diabetic mice had 86% more RANKL-positive chondrocytes on day 10 and 67% more on day 16 compared with the normoglycemic group

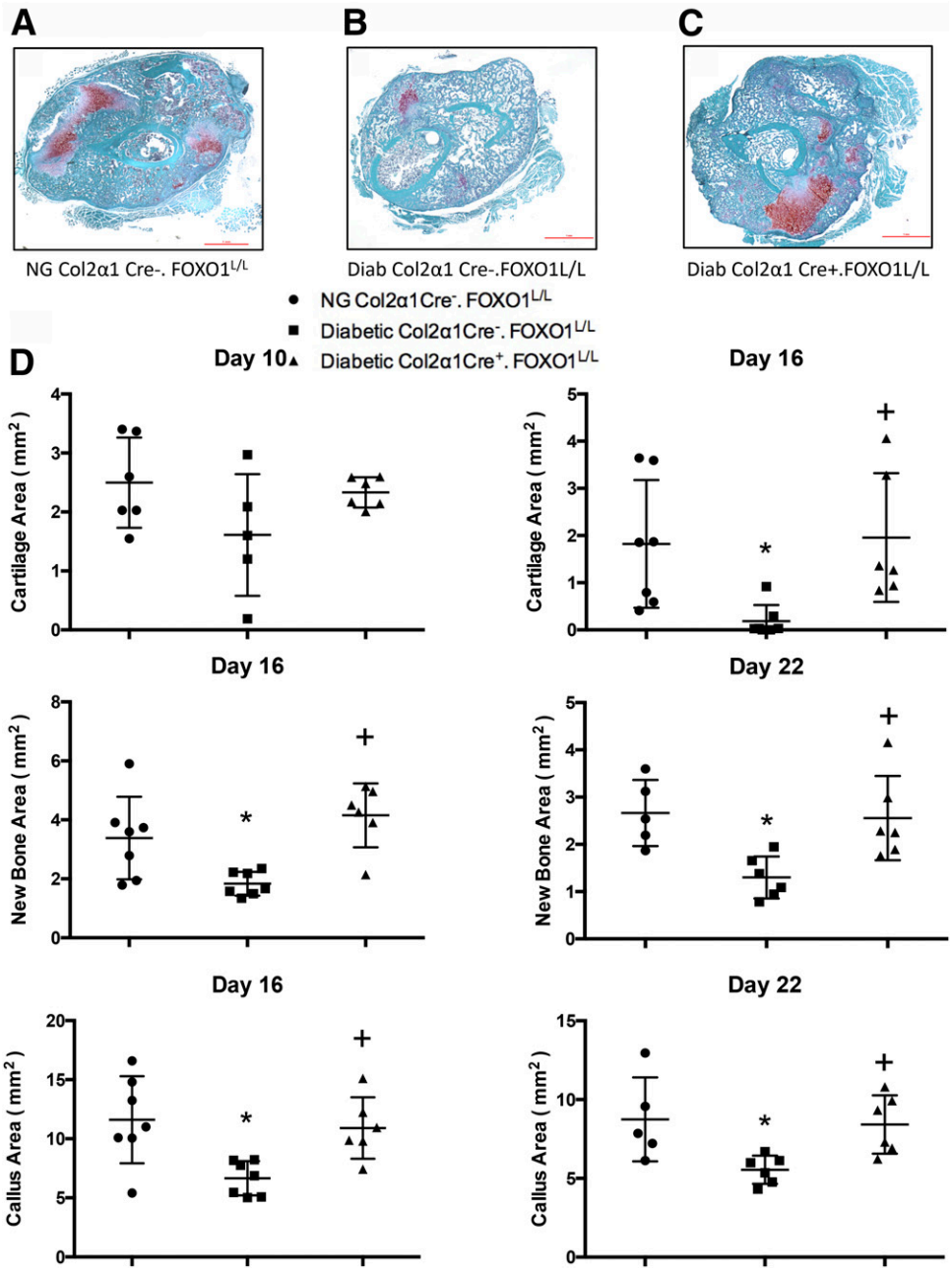

Figure 2— Diabetes significantly reduces the amount of cartilage and bone, which is rescued by FOXO1 deletion in chondrocytes. Histologic sections at the fracture site were obtained 16 days after fracture from normoglycemic (NG) Col2α1Cre^{-}.FOXO1$^{L/L}$ mice (*A*), diabetic (Diab) Col2α1Cre^{-}.FOXO1$^{L/L}$ mice (*B*), and diabetic (Diab) Col2α1Cre^{+}.FOXO1$^{L/L}$ (*C*) mice with FOXO1 deletion and stained with Safranin-O/fast green. The callus was defined as the area within the peripheral fibrous capsule, excluding the original cortical bone. Cartilage is stained red. Scale bar = 1 mm. *D*: Safranin-O/fast green–stained sections from the fracture site were examined for cartilage area 10 and 16 days after fracture, bone area 16 and 22 days after fracture, and total callus size 16 and 22 days after fracture. Data are expressed as mean ± SD; n = 5–7/group. Significance was determined by ANOVA followed by Tukey post hoc test ($P < 0.05$). *Significant difference between specimens from diabetic and matched NG animals; +significant difference between specimens from diabetic Col2α1Cre^{+}.FOXO1$^{L/L}$ and Col2α1Cre^{-}.FOXO1$^{L/L}$ mice.

($P < 0.05$) (Fig. 5*D*). Deletion of FOXO1 reduced the number of RANKL-expressing chondrocytes in diabetic mice ($P < 0.05$), even to a level below that of normoglycemic control littermates (Fig. 5*D*). RANKL mRNA levels were measured in the healing callus by quantitative PCR. There was a threefold increase in RANKL mRNA levels in diabetic mice compared with normoglycemic controls ($P < 0.05$) (Fig. 5*E*). In contrast, calluses from diabetic mice with ablated FOXO1 had significantly less mRNA ($P < 0.05$) (Fig. 5*E*).

To more directly assess the role of FOXO1 in regulating chondrocyte RANKL expression, primary chondrocytes were isolated from Col2α1Cre^{+}.FOXO1$^{L/L}$ and control

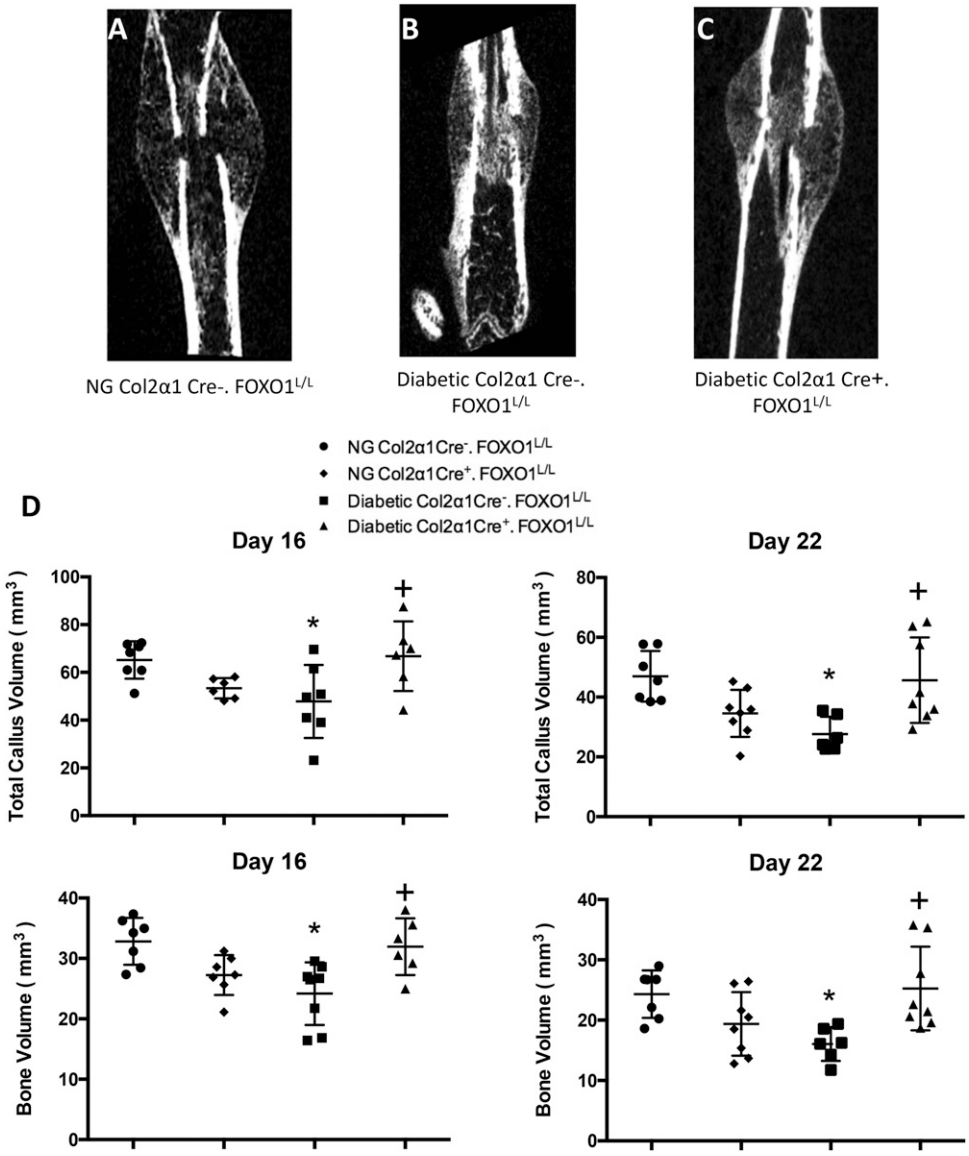

Figure 3—Diabetes impairs bone formation during fracture healing, which is rescued by FOXO1 deletion in chondrocytes. Micro-CT was performed on fracture calluses during healing 22 days after fracture in animals from normoglycemic (NG) Col2α1Cre^{-}.FOXO1$^{L/L}$ mice (*A*), diabetic Col2α1Cre^{-}.FOXO1$^{L/L}$ (*B*) mice, and diabetic Col2α1Cre^{+}.FOXO1$^{L/L}$ mice (*C*) with FOXO1 deletion. *D*: The callus volume and amount of bone volume were quantified in micro-CT images from mice 16 and 22 days after fracture. Data are expressed as mean ± SD; n = 6–8/group. Significance was determined by ANOVA followed by Tukey post hoc test ($P < 0.05$). *Significant difference between specimens from diabetic and matched NG animals; +significant difference between specimens from diabetic Col2α1Cre^{+}.FOXO1$^{L/L}$ and Col2α1Cre^{-}.FOXO1$^{L/L}$ mice.

Col2α1Cre^{-}.FOXO1$^{L/L}$ littermates. RANKL mRNA levels were reduced by 47% in chondrocytes from experimental mice under basal conditions, 37% less after serum stimulation, and 54% less after maturation to hypertrophic chondrocytes ($P < 0.05$) (Fig. 5*F*). Primary chondrocytes were also cultured in low and HG or with an advanced glycation end product (AGE), 200 μg/mL CML-albumin, or unmodified albumin (BSA) and RANKL levels assessed by immunofluorescence measuring mean fluorescence intensity. HG (25 mmol/L) and AGEs stimulated a 2.5–3-fold increase in RANKL compared with matched controls. The level of RANKL stimulated by HG or an AGE was returned to baseline levels in primary chondrocytes with ablated FOXO1 ($P < 0.05$) (Fig. 5*G*).

ChIP investigated FOXO1 interaction with the *RANKL* promoter. HG media stimulated a sevenfold enrichment of FOXO1 association with the RANKL promoter compared with low glucose media. Similarly, incubation with AGE (CML-BSA) induced a 13-fold enrichment of FOXO1 with the *RANKL* promoter. Incubation with osmotic control (mannitol) had no significant effect, which indicates that the increase in RANKL activities was due to the effect of diabetic conditions, HG and AGEs (Fig. 6*A*).

Overexpression of FOXO1 stimulated a twofold increase in RANKL promoter activity when ATDC5 cells were cultured in low glucose media (Fig. 6*B*). Culturing the ATDC5 cells in HG media or AGE caused an additional

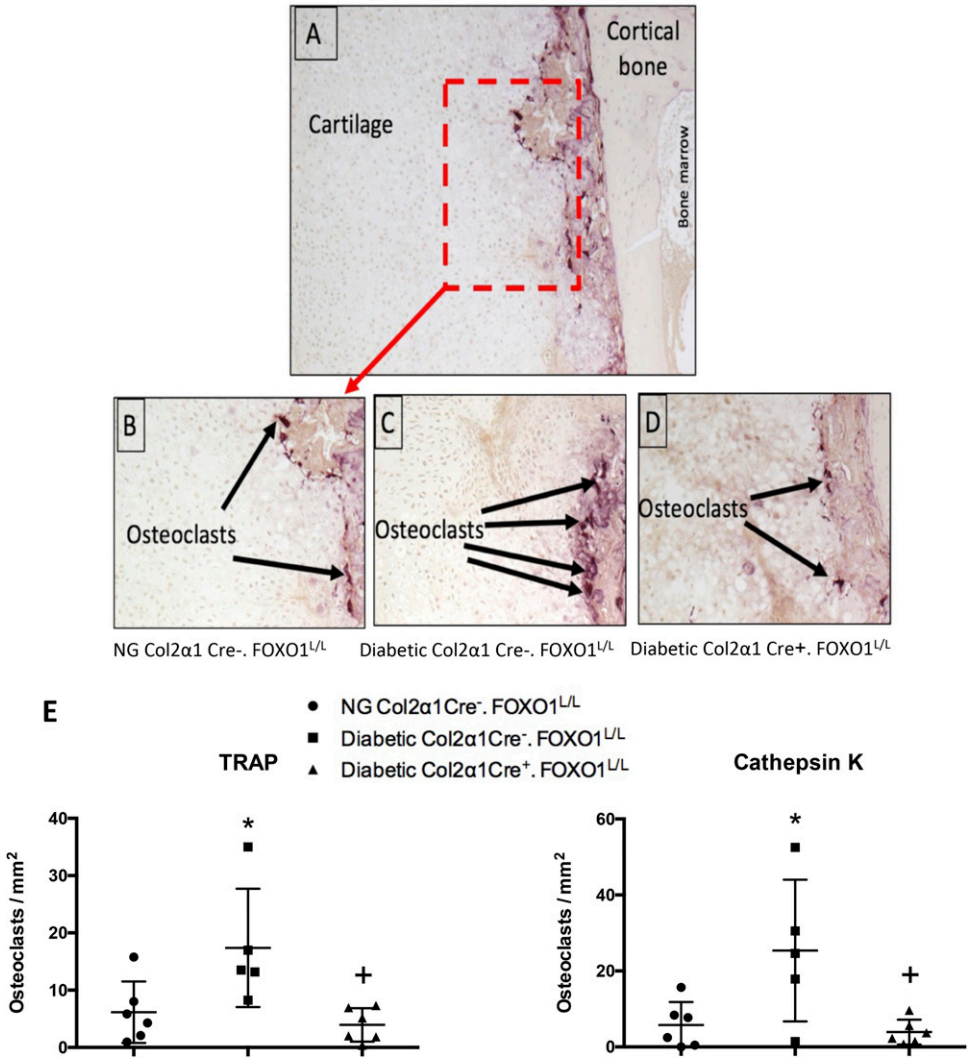

Figure 4—FOXO1 deletion in chondrocytes rescues the increase in osteoclasts caused by diabetes. Histologic sections were obtained 10 days after fracture from normoglycemic (NG) Col2α1Cre^{-}.FOXO1$^{L/L}$ mice, diabetic Col2α1Cre^{-}.FOXO1$^{L/L}$ mice, or diabetic Col2α1Cre^{+}.FOXO1$^{L/L}$ mice with FOXO1 deletion. Sections were stained for TRAP. Original magnification ×100 (*A*) and ×200 (*B–D*). *E*: Osteoclasts adjacent to cartilage were counted as multinucleated TRAP-positive cells or cathepsin K–positive cells determined by immunohistochemistry with antibody specific to cathepsin K ($n = 5$ to 6). Data are expressed as mean ± SD; $n = 5$ to 6/group. Significance was determined by ANOVA followed by Tukey post hoc test ($P < 0.05$). *Significant difference between specimens from diabetic and matched NG animals; +significant difference between specimens from diabetic Col2α1Cre^{+}.FOXO1$^{L/L}$ and Col2α1Cre^{-}.FOXO1$^{L/L}$ mice.

~80% increase in RANKL promoter activity in ATDC5 cells transfected with a FOXO1 expression vector (Fig. 6*B*).

FOXO1 Nuclear Localization Stimulated by HG and AGE Is Inhibited by Insulin, TLR4 Inhibitor, Histone Deacetylase Inhibitor, NAC, and L-NAME but Not AKT Inhibitor

FACS was used to assess the activation of FOXO1 as measured by nuclear localization following stimulation by HG, AGEs, or HG plus AGEs. HG stimulated a fourfold increase in FOXO1 nuclear localization, AGEs a 4.5-fold increase, and the combination of HG and AGEs resulted in a 5.5-fold increase in FOXO1 nuclear localization (Fig. 6*C*). Insulin treatment rescued the effect of HG, AGEs, and HG plus AGEs on FOXO1 activation to normal levels ($P < 0.05$). Additionally, TLR4 inhibitor, histone deacetylase inhibitor, NAC, and L-NAME resulted in blocking the effect of the HG, AGEs, and the combination of HG and AGEs on FOXO1 nuclear localization ($P < 0.05$). In contrast, an AKT inhibitor had no effect on FOXO1 activation derived by HG and AGEs ($P > 0.05$) (Fig. 6*C*). Thus, HG and AGEs as well as the combination of both stimulate FOXO1 activation through well-established pathways and are inhibited by insulin stimulation.

DISCUSSION

Individuals with diabetes are at higher risk of bone fracture (29–31). Moreover, studies in humans and animals demonstrate that diabetes impairs and delays the healing

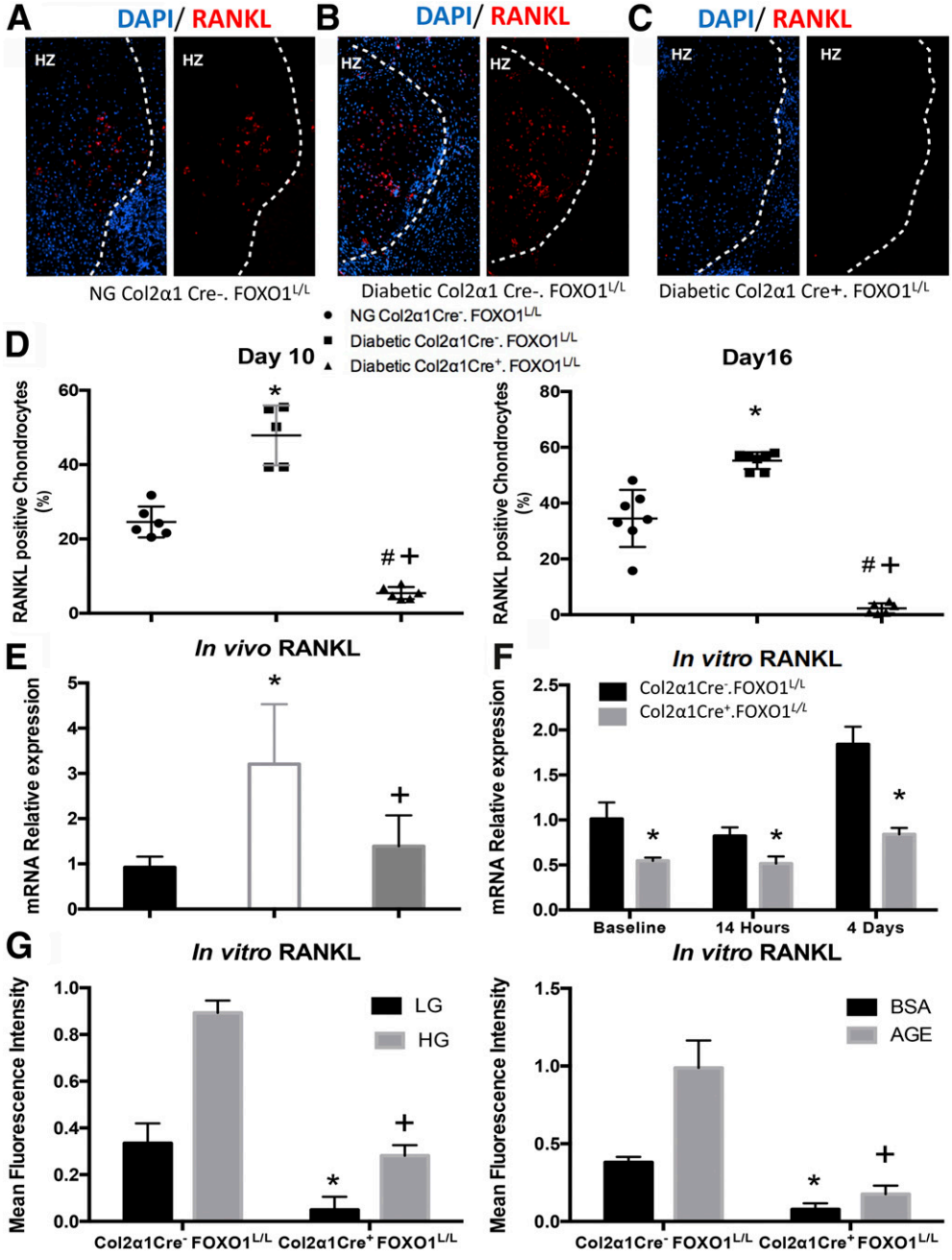

Figure 5—Diabetes increases chondrocytes' RANKL expression, which is FOXO1 dependent. Histologic sections were obtained 10 days after fracture from normoglycemic (NG) Col2α1Cre^{-}.FOXO1$^{L/L}$ mice (*A*), diabetic Col2α1Cre^{-}.FOXO1$^{L/L}$ mice (*B*), or diabetic Col2α1Cre^{+}.FOXO1$^{L/L}$ mice (*C*) with FOXO1 deletion. Immunofluorescence was carried out with antibody specific for RANKL, and no signal was detected with matched control antibody (not shown). Nuclei were stained with DAPI. The white dashed line marks the hypertrophic cartilage zone (HZ). Original magnification ×200. *D*: The percentage of RANKL-positive chondrocytes in the hypertrophic zone was counted in immunofluorescent images with antibody specific to RANKL from specimens obtained 10 and 16 days after fracture. *E*: RNA was obtained from fracture calluses 10 days after fracture, and RANKL mRNA levels were quantified by real-time PCR for NG Col2α1Cre^{-}.FOXO1$^{L/L}$ (black bar), diabetic Col2α1Cre^{-}.FOXO1$^{L/L}$ (white bar), and diabetic Col2α1Cre^{+}.FOXO1$^{L/L}$ (gray bar) mice (n = 5 to 6/group). *D* and *E*: *Significant difference between specimens from diabetic and NG Col2α1Cre^{-}.FOXO1$^{L/L}$ mice; +significant difference between specimens from diabetic Col2α1Cre^{+}.FOXO1$^{L/L}$ and Col2α1Cre^{-}.FOXO1$^{L/L}$ mice; #significant difference between the diabetic Col2α1Cre^{+}.FOXO1$^{L/L}$ and NG Col2α1Cre^{-}.FOXO1$^{L/L}$ mice. For each comparison significance was determined by ANOVA followed by Tukey post hoc test ($P < 0.05$). *F*: Primary chondrocytes were isolated from the control Col2α1Cre^{-}.FOXO1$^{L/L}$ and experimental Col2α1Cre^{+}.FOXO1$^{L/L}$ mice and grown to confluence. They were then incubated in standard media with serum for 14 h or cultured in chondrogenic media for 4 days. RNA was obtained, and RANKL mRNA levels were measured by real-time PCR. *Significant difference between cells obtained from Col2α1Cre^{+}.FOXO1$^{L/L}$ and Col2α1Cre^{-}.FOXO1$^{L/L}$ determined by Student t test ($P < 0.05$). *G*: Primary chondrocytes were isolated from Col2α1Cre^{-}.FOXO1$^{L/L}$ and Col2α1Cre^{+}.FOXO1$^{L/L}$ and incubated in standard media with low glucose (LG), HG, CML-BSA, advanced AGE, or unmodified BSA. RANKL was detected by immunofluorescence with antibody specific for RANKL, and no signal was detected with matched control antibody (not shown). Nuclei were stained with DAPI. * and + indicate a significant difference between the control and FOXO1-deleted chondrocytes under the same conditions by Student t test ($P < 0.05$).

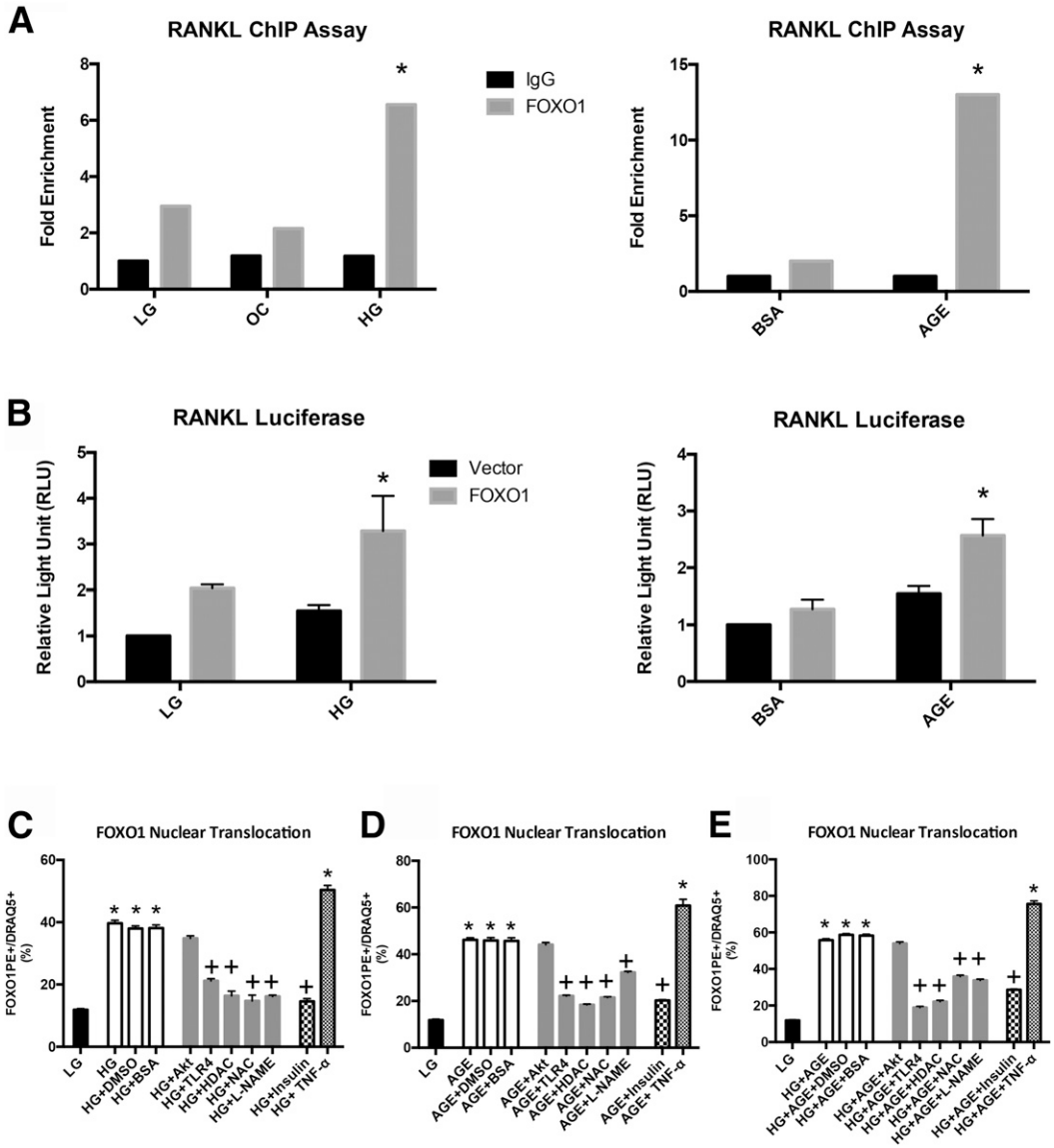

Figure 6—FOXO1 nuclear localization, FOXO1 interaction with the RANKL promoter, and FOXO1-induced RANKL promoter activity in chondrocytes are stimulated by HG and an advanced AGE. *A*: Chondrocytes were incubated in standard media or media supplemented with HG (25 mmol/L) or osmotic control (OC), 25 mmol/L mannitol for 5 days, or 200 μg/mL CML-BSA, an AGE, or unmodified BSA for 3 days. ChIPs were performed by pulldown with FOXO1-specific antibody or matched control IgG. *B*: Chondrocytes were cotransfected with a FOXO1 expression plasmid and a RANKL luciferase reporter construct and incubated in standard media or media supplemented with HG or an AGE as above. Luciferase activity was measured and normalized by Renilla control. *C*: FOXO1 nuclear localization was measured by flow cytometry in chondrocytes cultured with standard glucose (LG) vs. HG for 5 days and compared with positive control, cells incubated in TNF-α (10 ng/mL) for 1 h. For the last 24 h, cells were incubated with the following inhibitors: 1L6-hydroxymethyl-chiro-inositol-2-(R)-2-*O*-methyl-3-*O*-octadecyl-sn-glycerocarbonate, an AKT inhibitor; TAK242, a TLR4 inhibitor; trichostatin A, a deacetylase inhibitor; NAC, an antioxidant; L-NAME, a nitric oxide synthase inhibitor; or insulin. *D*: FOXO1 nuclear localization was measured in chondrocytes stimulated with AGE, CML-BSA, or unmodified BSA for 3 days and compared with positive control, TNF-α. For the last 24 h, cells were incubated with inhibitors as described for *C*. *E*: FOXO1 nuclear translocation was measured by flow cytometry in chondrocytes incubated in HG for 5 days plus an AGE, CML-BSA, or unmodified BSA for 3 days and compared with cells incubated in TNF-α, a positive control. For the last 24 h, cells were incubated with inhibitors as described for *C*. Data are expressed as mean ± SEM. *Significant difference compared with standard media (LG) determined by ANOVA followed by Tukey post hoc test ($P < 0.001$); +significant difference compared with HG+AGE group determined by ANOVA followed by Tukey post hoc test ($P < 0.001$).

process (32,33). We found that the impact of diabetes on chondrocytes plays a paramount role in impaired fracture healing. The results also confirm that diabetes causes the accelerated loss of cartilage and demonstrates for the first time that this is directly modulated by chondrocytes through a mechanism that involves the transcription factor FOXO1. Although it is recognized that diabetes has a detrimental effect on fracture healing due to the effect on osteoblasts (34,35), our results indicate that chondrocytes are also strongly affected by diabetes and

have a dramatic effect on the healing response. Diabetic animals had a striking decrease in cartilage during the phase of endochondral bone formation and subsequently had reduced bone formation. Both effects were reversed by lineage-specific deletion of FOXO1 in chondrocytes. This result establishes the importance of chondrocytes in understanding how diabetes alters fracture repair and identifies FOXO1 as a key mechanism.

Cartilage provides an anlage for endochondral bone formation, which is critical for fracture stability. We found little difference in the cartilage area between diabetic and normoglycemic groups at 10 days postfracture, consistent with previous reports (36). However, during endochondral bone formation, cartilage was rapidly lost in the diabetic group on day 16, and diabetes significantly reduced subsequent bone formation measured in the callus histologically and radiographically. Diabetes-enhanced osteoclast formation accounted for the reduced cartilage in the diabetic group, assessed both by TRAP-positive and cathepsin K–positive osteoclasts lining cartilage. Chondrocyte deletion of FOXO1 rescued the increase in osteoclasts caused by diabetes. The increase in osteoclasts that we observed in diabetic mice has also been observed in humans. Suzuki et al. (37) reported that patients with diabetes had higher TRAP serum levels indicative of increased bone resorption compared with healthy individuals. They have also indicated that those patients with diabetes had higher concentrations of type 1 collagen cross-linked carboxy-terminal telopeptide in their urine, which confirms the increased resorption rate (37). It has been also reported that different inflammatory cytokines are involved in osteoclast activation. The accelerated cartilage resorptions in the current investigation may be explained mechanistically by the increased number of osteoclasts in the healing callus, which is linked to FOXO1-mediated RANKL expression.

To better understand how diabetes enhanced osteoclast formation, we examined RANKL expression in chondrocytes. Diabetic animals had almost two times more chondrocytes expressing RANKL in the healing callus compared with the normoglycemic control group. Diabetes-enhanced RANKL expression was reversed upon FOXO1 deletion. It has previously been reported that patients with type 1 diabetes have increased total soluble RANKL (38). This is consistent with our results in mice, which suggest that diabetes dysregulates RANKL expression in chondrocytes to affect the transition from cartilage to bone. Moreover, RANKL secreted by chondrocytes supports the differentiation of precursors to osteoclasts (39). Furthermore, previous studies have demonstrated that HG enhances formation of osteoclasts (40). Our studies identify an important mechanism through which FOXO1 is stimulated by factors present in diabetes, HG and AGEs, to promote the expression of RANKL in chondrocytes. Moreover, HG and AGE stimulation increased RANKL promoter activity and stimulated a direct interaction of FOXO1 with the RANKL promoter.

We examined potential mechanisms through which two factors that are known to be elevated in diabetes, HG or stimulation by an AGE, induced FOXO1 nuclear localization, a critical initial step in its activation. Both HG and CML-BSA stimulated a fourfold increase in FOXO1 nuclear localization, which was close to the fivefold stimulation induced by TNF-α. Insulin blocked both HG- and AGE-stimulated FOXO1 nuclear localization, demonstrating that low insulin levels or insulin resistance in chondrocytes are important in facilitating FOXO1 activation. However, an Akt inhibitor alone had no effect, suggesting that HG or AGE stimulation did not induce a FOXO1 inhibitory pathway through Akt. Pathways previously shown to mediate the effect of HG or AGEs were investigated to determine whether they mediated the effect of HG or AGEs. It has been reported that HG induces TLR4 activation in endothelial cells and modulates FOXO1 activation in myeloid cells via a TLR4 pathway (41,42). Inhibition of TLR4 reduced the effect of HG and AGE stimulation by 46–66%. A deacetylase inhibitor (tyramide signal amplification), which has been shown to reduce FOXO1 activity in hepatocytes (43), reduced FOXO1 nuclear localization in chondrocytes stimulated by HG and AGEs by ∼60%. The antioxidant NAC, which has been reported to reduce FOXO1 activation stimulated by TNF-α (44), and L-NAME, a nitric oxide synthase inhibitor that has been reported to reduce AGE-induced fibroblast apoptosis mediated by FOXO1 (45), both reduced FOXO1 nuclear localization by ∼30–60%. Taken together, these studies indicate that HG and an AGE both stimulate FOXO1 nuclear localization through multiple pathways that involve acetylation, reactive oxygen species, nitric oxide synthase, and TLR4 activity. Each of these has been shown to be important in FOXO1 stimulation in other cell types. Moreover, insulin, which is known to inhibit FOXO1 nuclear localization, was effective in blocking FOXO1 activation in chondrocytes stimulated by an AGE or HG environment.

FOXOs are key regulators of cellular homeostasis, stress response, longevity, and wound healing (46). FOXOs maintain stem cell populations via oxidative stress resistance and transcriptional regulation of cell cycle arrest (47). Lineage-specific FOXO1 ablation in mature osteoblasts mediated by collagen-1α1–regulated Cre recombinase has been reported to reduce osteoblast numbers, bone volume, and bone mineral density, indicating that FOXO1 in osteoblasts is a positive regulator of bone formation (48). However, simultaneous deletion of FOXO1, FOXO3, and FOXO4 by osterix-driven Cre-recombinase in osteoblast/adipocyte progenitors has the opposite effect, suggesting that the combined FOXOs in these progenitors suppress bone formation and favor adipocity (49). The previous findings as well as those reported in this study highlight the pivotal role of FOXO1 in skeletal bone formation, homeostasis, and repair (50).

In summary, we found that specific deletion of FOXO1 in chondrocytes reversed diabetes-impaired fracture healing. These studies point to the impact that diabetes has on

chondrocytes and their role in propagating a negative effect on eventual endochondral bone formation in the fracture-healing process. Moreover, the data identify a specific mechanism, FOXO1-driven RANKL expression, as a key component through which conditions present in diabetes, HG and AGEs, can directly modulate FOXO1 activity to alter gene expression to negatively affect the repair process.

Funding. This work was supported by funding from National Institutes of Health grants R01-AR-060055, R01-DE-017732, and R01-AR-069044.

Duality of Interest. No potential conflicts of interest relevant to this article were reported.

Author Contributions. M.A.A. designed and carried out experiments, interpreted data, and wrote the manuscript. C.Z. assisted in experimental design, carried out experiments, and interpreted data. C.L. assisted in experimental design and carried out experiments. T.N.M. carried out experiments and edited the manuscript. L.Y. carried out experiments. J.D.R. carried out experiments. H.J. carried out experiments. G.D. carried out experiments. J.P.O. assisted in experimental design and edited the manuscript. D.T.G. designed experiments, interpreted data, and wrote the manuscript. D.T.G. is the guarantor of this work and, as such, had full access to all of the data in the study and takes responsibility for the integrity of the data and the accuracy of the data analysis.

References

1. Gerstenfeld LC, Cullinane DM, Barnes GL, Graves DT, Einhorn TA. Fracture healing as a post-natal developmental process: molecular, spatial, and temporal aspects of its regulation. J Cell Biochem 2003;88:873–884
2. Lee FY, Choi YW, Behrens FF, DeFouw DO, Einhorn TA. Programmed removal of chondrocytes during endochondral fracture healing. J Orthop Res 1998;16:144–150
3. Grcevic D, Pejda S, Matthews BG, et al. In vivo fate mapping identifies mesenchymal progenitor cells. Stem Cells 2012;30:187–196
4. Sandberg M, Tamminen M, Hirvonen H, Vuorio E, Pihlajaniemi T. Expression of mRNAs coding for the alpha 1 chain of type XIII collagen in human fetal tissues: comparison with expression of mRNAs for collagen types I, II, and III. J Cell Biol 1989;109:1371–1379
5. Barnes GL, Kostenuik PJ, Gerstenfeld LC, Einhorn TA. Growth factor regulation of fracture repair. J Bone Miner Res 1999;14:1805–1815
6. Jonsson H, Allen P, Peng SL. Inflammatory arthritis requires Foxo3a to prevent Fas ligand-induced neutrophil apoptosis. Nat Med 2005;11:666–671
7. Bahney CS, Hu DP, Taylor AJ, et al. Stem cell-derived endochondral cartilage stimulates bone healing by tissue transformation. J Bone Miner Res 2014;29:1269–1282
8. Zhou X, von der Mark K, Henry S, Norton W, Adams H, de Crombrugghe B. Chondrocytes transdifferentiate into osteoblasts in endochondral bone during development, postnatal growth and fracture healing in mice. PLoS Genet 2014;10:e1004820
9. Praemer A, Rice D. *Musculoskeletal Conditions in the United States*. Rosemont, IL, American Academy of Orhtopedic Surgeons, 1992, p. 85–124
10. Kagel EM, Einhorn TA. Alterations of fracture healing in the diabetic condition. Iowa Orthop J 1996;16:147–152
11. Dabelea D, Mayer-Davis EJ, Saydah S, et al.; SEARCH for Diabetes in Youth Study. Prevalence of type 1 and type 2 diabetes among children and adolescents from 2001 to 2009. JAMA 2014;311:1778–1786
12. Mayer-Davis EJ, Dabelea D, Lawrence JM. Incidence trends of type 1 and type 2 diabetes among youths, 2002-2012. N Engl J Med 2017;377:301
13. Weber DR, Haynes K, Leonard MB, Willi SM, Denburg MR. Type 1 diabetes is associated with an increased risk of fracture across the life span: a population-based cohort study using The Health Improvement Network (THIN). Diabetes Care 2015;38:1913–1920
14. Maddaloni E, D'Eon S, Hastings S, et al. Bone health in subjects with type 1 diabetes for more than 50 years. Acta Diabetol 2017;54:479–488
15. Botushanov NP, Orbetzova MM. Bone mineral density and fracture risk in patients with type 1 and type 2 diabetes mellitus. Folia Med (Plovdiv) 2009;51:12–17
16. Stolzing A, Sellers D, Llewelyn O, Scutt A. Diabetes induced changes in rat mesenchymal stem cells. Cells Tissues Organs 2010;191:453–465
17. Sheweita SA, Khoshhal KI. Calcium metabolism and oxidative stress in bone fractures: role of antioxidants. Curr Drug Metab 2007;8:519–525
18. Ponugoti B, Dong G, Graves DT. Role of forkhead transcription factors in diabetes-induced oxidative stress. Exp Diabetes Res 2012;2012:939751
19. Caramés B, Kiosses WB, Akasaki Y, et al. Glucosamine activates autophagy in vitro and in vivo. Arthritis Rheum 2013;65:1843–1852
20. Graves DT, Naguib G, Lu H, Leone C, Hsue H, Krall E. Inflammation is more persistent in type 1 diabetic mice. J Dent Res 2005;84:324–328
21. Like AA, Rossini AA. Streptozotocin-induced pancreatic insulitis: new model of diabetes mellitus. Science 1976;193:415–417
22. Gerstenfeld LC, Wronski TJ, Hollinger JO, Einhorn TA. Application of histomorphometric methods to the study of bone repair. J Bone Miner Res 2005;20:1715–1722
23. Kayal RA, Tsatsas D, Bauer MA, et al. Diminished bone formation during diabetic fracture healing is related to the premature resorption of cartilage associated with increased osteoclast activity. J Bone Miner Res 2007;22:560–568
24. Bouxsein ML, Boyd SK, Christiansen BA, Guldberg RE, Jepsen KJ, Müller R. Guidelines for assessment of bone microstructure in rodents using micro-computed tomography. J Bone Miner Res 2010;25:1468–1486
25. Mirando AJ, Dong Y, Kim J, Hilton MJ. Isolation and culture of murine primary chondrocytes. Methods Mol Biol 2014;1130:267–277
26. Alikhani M, Roy S, Graves DT. FOXO1 plays an essential role in apoptosis of retinal pericytes. Mol Vis 2010;16:408–415
27. Zhang C, Ponugoti B, Tian C, et al. FOXO1 differentially regulates both normal and diabetic wound healing. J Cell Biol 2015;209:289–303
28. O'Brien CA, Kern B, Gubrij I, Karsenty G, Manolagas SC. Cbfa1 does not regulate RANKL gene activity in stromal/osteoblastic cells. Bone 2002;30:453–462
29. Ivers RQ, Cumming RG, Mitchell P, Peduto AJ; Blue Mountains Eye Study. Diabetes and risk of fracture: The Blue Mountains Eye Study. Diabetes Care 2001;24:1198–1203
30. Nicodemus KK, Folsom AR; Iowa Women's Health Study. Type 1 and type 2 diabetes and incident hip fractures in postmenopausal women. Diabetes Care 2001;24:1192–1197
31. Vestergaard P, Rejnmark L, Mosekilde L. Relative fracture risk in patients with diabetes mellitus, and the impact of insulin and oral antidiabetic medication on relative fracture risk. Diabetologia 2005;48:1292–1299
32. Loder RT. The influence of diabetes mellitus on the healing of closed fractures. Clin Orthop Relat Res 1988;232:210–216
33. Herskind AM, Christensen K, Nørgaard-Andersen K, Andersen JF. Diabetes mellitus and healing of closed fractures. Diabete Metab 1992;18:63–64
34. Sellmeyer DE, Civitelli R, Hofbauer LC, Khosla S, Lecka-Czernik B, Schwartz AV. Skeletal metabolism, fracture risk, and fracture outcomes in type 1 and type 2 diabetes. Diabetes 2016;65:1757–1766
35. Kalaitzoglou E, Popescu I, Bunn RC, Fowlkes JL, Thrailkill KM. Effects of type 1 diabetes on osteoblasts, osteocytes, and osteoclasts. Curr Osteoporos Rep 2016;14:310–319
36. Alblowi J, Kayal RA, Siqueira M, et al. High levels of tumor necrosis factor-alpha contribute to accelerated loss of cartilage in diabetic fracture healing [published correction appears in Am J Pathol 2009;175:2249]. Am J Pathol 2009;175:1574–1585
37. Suzuki K, Kurose T, Takizawa M, et al. Osteoclastic function is accelerated in male patients with type 2 diabetes mellitus: the preventive role of osteoclastogenesis inhibitory factor/osteoprotegerin (OCIF/OPG) on the decrease of bone mineral density. Diabetes Res Clin Pract 2005;68:117–125

38. Tsentidis C, Gourgiotis D, Kossiva L, et al. Higher levels of s-RANKL and osteoprotegerin in children and adolescents with type 1 diabetes mellitus may indicate increased osteoclast signaling and predisposition to lower bone mass: a multivariate cross-sectional analysis. Osteoporos Int 2016;27:1631–1643
39. Martínez-Calatrava MJ, Prieto-Potín I, Roman-Blas JA, Tardio L, Largo R, Herrero-Beaumont G. RANKL synthesized by articular chondrocytes contributes to juxta-articular bone loss in chronic arthritis. Arthritis Res Ther 2012;14:R149
40. Reni C, Mangialardi G, Meloni M, Madeddu P. Diabetes stimulates osteoclastogenesis by acidosis-induced activation of transient receptor potential cation channels. Sci Rep 2016;6:30639
41. Wang L, Wang J, Fang J, Zhou H, Liu X, Su SB. High glucose induces and activates Toll-like receptor 4 in endothelial cells of diabetic retinopathy. Diabetol Metab Syndr 2015;7:89
42. Dong G, Song L, Tian C, et al. FOXO1 regulates bacteria-induced neutrophil activity. Front Immunol 2017;8:1088
43. Mihaylova MM, Vasquez DS, Ravnskjaer K, et al. Class IIa histone deacetylases are hormone-activated regulators of FOXO and mammalian glucose homeostasis. Cell 2011;145:607–621
44. Kayal RA, Siqueira M, Alblowi J, et al. TNF-α mediates diabetes-enhanced chondrocyte apoptosis during fracture healing and stimulates chondrocyte apoptosis through FOXO1. J Bone Miner Res 2010;25:1604–1615
45. Alikhani M, Maclellan CM, Raptis M, Vora S, Trackman PC, Graves DT. Advanced glycation end products induce apoptosis in fibroblasts through activation of ROS, MAP kinases, and the FOXO1 transcription factor. Am J Physiol Cell Physiol 2007;292:C850–C856
46. Wang Y, Zhou Y, Graves DT. FOXO transcription factors: their clinical significance and regulation. BioMed Res Int 2014;2014:925350
47. Paik JH, Ding Z, Narurkar R, et al. FoxOs cooperatively regulate diverse pathways governing neural stem cell homeostasis. Cell Stem Cell 2009;5:540–553
48. Rached MT, Kode A, Xu L, et al. FoxO1 is a positive regulator of bone formation by favoring protein synthesis and resistance to oxidative stress in osteoblasts. Cell Metab 2010;11:147–160
49. Iyer S, Ambrogini E, Bartell SM, et al. FOXOs attenuate bone formation by suppressing Wnt signaling. J Clin Invest 2013;123:3409–3419
50. Kousteni S. FoxO1, the transcriptional chief of staff of energy metabolism. Bone 2012;50:437–443